Toward the Detection and Imaging of Ocean Microplastics With a Spaceborne Radar

Madeline C. Evans and Christopher S. Ruf, *Fellow, IEEE*

***Abstract*— Ocean microplastic concentrations are known to vary significantly by location, with especially high levels in the North Atlantic and North Pacific gyres. Most direct measurements come from plankton net trawling made in these regions; concentrations in other regions have been estimated by microplastic transport models that depend on large-scale ocean circulation patterns. However, global measurements of microplastic distribution and its temporal variability are lacking. A new method is presented for detecting and imaging the global distribution of ocean microplastics from space. The method uses spaceborne bistatic radar measurements of ocean surface roughness and relies on an assumed reduction in responsiveness to wind-driven roughening caused by surfactants that act as tracers for microplastics near the surface. Annual mean microplastic distributions estimated by the radars are generally consistent with model predictions. The spaceborne observations are also able to detect temporal changes that are not resolved by the models. For example, seasonal dependencies are observed at mid-latitudes in both Northern and Southern Hemispheres, with lower concentrations noted in the winter months. Time lapse images at finer spatial and temporal scales reveal episodic bursts of microplastic tracers in the outflow from major river discharges into the sea. This new method will provide better monitoring of ocean microplastics and will support future model development and validation.**

***Index Terms*— GNSS data, miscellaneous applications, oceans and water.**

I. Introduction and Motivation

ANNUAL global production of plastic has increased every year since the 1950s, reaching 359 million metric tons in 2018 [1], [2]. This trend in conjunction with inadequate waste management infrastructure and practices results in unsecure plastic debris disposal (e.g., open, uncontrolled landfills) [3]. Mismanaged plastics are more likely to be carried to river drainage zones that subsequently distribute into the world's oceans [3]–[5]. The presence of plastic debris in the ocean was first documented in the 1970s [6], and estimates show plastic now accounts for 80%–85% of marine litter [7]. Plastics rarely biodegrade; rather they break down via solar UV radiation and wave mechanics into smaller particles called microplastics [4], [7]–[10].

Most ocean plastic concentration data come from plankton net trawling [10], [11]. However, net trawling has a low sample rate and design flaws that may be underestimating true plastic concentrations [4], [9]. Plastic concentrations are also not well sampled outside of the North Atlantic and North Pacific gyres [9], [10]. In addition, the rate of redistribution of plastics in the ocean varies widely. Estimates of their drift velocity can exceed 1 m/s under persistent, moderate wind conditions, resulting in transport of ∼100 km/day [12]. Furthermore, concentrations of plastic debris in close proximity can vary by more than three orders of magnitude in the span of 24 h [13]. This highlights the effects of complex transport mechanisms and spatiotemporal variability that net trawl sampling is unable to adequately resolve [13]–[15].

Remote sensing offers a means to help understand the dynamics of plastic transport and locate potential accumulation zones [15], [16]. The integration of remote sensing and *in situ* observations has been proposed as the next step in monitoring marine plastic pollution [16]. Remote-sensing methods, including optical sensing, synthetic aperture radar, hyperspectral imaging, and thermal infrared sensing, have the potential to either track plastics directly or infer plastic concentrations through proxy measurements. However, they have not yet been developed for widespread plastic detection in the open ocean [15]–[17]. An alternate approach is presented here with the potential to provide more global coverage and to resolve changes in microplastic distribution and transport dynamics on time scales of weeks to months.

II. Overview of Remote Sensing Approach

The detection of microplastics near the ocean surface is derived from measurements made by the CYGNSS low Earth orbiting bistatic radars, which are designed to measure wind speed above the ocean [18], [19]. The strength of radar reflections from the ocean depends on the wind-driven roughening of the surface. Radars used to measure winds rely on a nominal relationship between wind speed and ocean roughness [20], [21]. These satellite systems produce global maps of ocean winds, which are widely used for atmospheric and oceanographic applications [22], [23].

The radar measurements are repurposed here to estimate ocean microplastic concentrations by examining deviations of

Manuscript received February 16, 2021; revised April 16, 2021; accepted May 16, 2021. This work was supported by the National Aeronautics and Space Administration (NASA) Science Mission Directorate under Contract NNL13AQ00C. *(Corresponding author: Christopher S. Ruf.)*

Madeline C. Evans is with the Department of Electrical and Computer Engineering, University of Michigan, Ann Arbor, MI 48109 USA (e-mail: madevans@umich.edu).

Christopher S. Ruf is with the Department of Climate and Space Sciences and Engineering, University of Michigan, Ann Arbor, MI 48109 USA (e-mail: cruf@umich.edu).

This article has supplementary downloadable material available at https://doi.org/10.1109/TGRS.2021.3081691.

Digital Object Identifier 10.1109/TGRS.2021.3081691

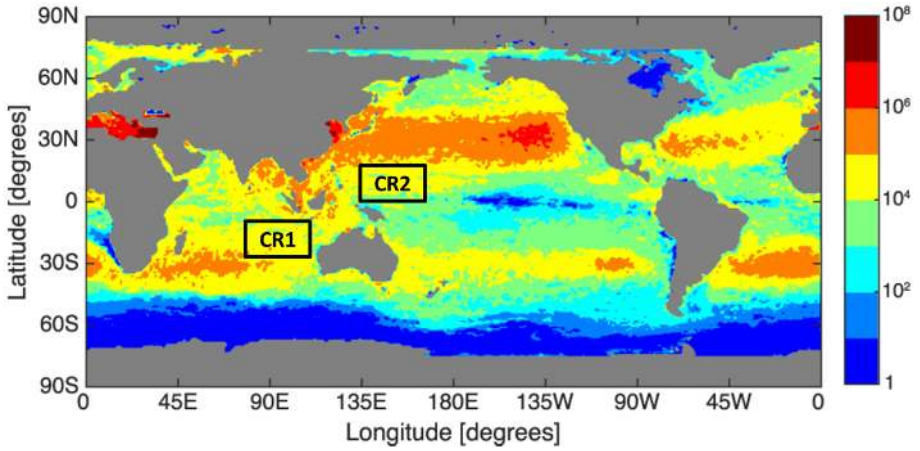

Fig. 1. Global distribution of ocean microplastic number density (#/km^2) predicted by van Sebille *et al.* [10], with the two control regions (CR1 and CR2) highlighted by black boxes. In these regions, ocean microplastic concentration, other damping factors, and the presence of atmospheric stability conditions affecting ocean surface roughness are all consistently low, resulting in characteristically high MSS anomalies. Radar measurements in these regions are used to define a baseline relationship between ocean surface wind speed and roughness against which anomalies are detected in other parts of the ocean.

the measured ocean roughness from the roughness predicted by a nominal relationship between it and ocean surface wind speed. Here, roughness is characterized by the mean square slope (MSS) of the surface height. In order to compare measured to predicted values, an independent source of wind speed is needed that is colocated with the measured roughness. The NOAA Global Data Assimilation System (GDAS) reanalysis product is used [24]. An estimate of MSS is made from the wind speed using an empirical model derived from a large population of colocated samples of wind and MSS in regions of the ocean believed to contain low concentrations of ocean microplastics [10]. The selected regions are outside of the intertropical convergence zone (ITCZ), where persistent anomalous atmospheric instability conditions can alter the responsiveness of the ocean surface to wind roughening. MSS anomaly, the difference between measured and predicted ocean surface roughness for a given wind speed, is used as an indicator of microplastic concentration. A negative anomaly indicates that the surface of the ocean was roughened less by the wind than it would have been had the microplastics not been present. The magnitude of the negative anomaly indicates the estimated concentration of microplastics present. The connection between MSS anomaly and ocean microplastic concentration may in fact be indirect, as discussed below.

The results presented below demonstrate a strong correlation between variations in ocean microplastic concentration and MSS anomaly. We hypothesize that the presence of ocean microplastics is accompanied by surfactant tracers, and that surfactant wave damping is causing the observed reduction in responsiveness of the surface to wind-driven roughening. Surfactants are ubiquitous in marine environments, and their damping properties in relation to gravity-capillary waves have been studied [25]–[27]. Additionally, surfactants are known to accumulate in ocean convergence zones along with microplastics [15], so it is not unreasonable to assume their transport mechanisms may be similar. Floating material in the ocean, including plastic particles, surfactants, oils, and marine organisms can aggregate in common locations when surface currents transport buoyant matter to the boundaries between converging fronts [15], [28]. There is also evidence that increased concentrations of surfactants in wastewater facilities may significantly increase microplastic concentrations in effluents [29]. While these relationships suggest that surfactants may act as tracers of surface-level microplastics from their sources to the accumulation zones, future investigations are needed into the similarities and differences of microplastic and surfactant transport dynamics and into confounding factors affecting wave suppression to fully validate our hypothesis.

III. Description of Data and Models

CYGNSS Level 2, Version 2.1 wind speed data (time-tagged, 25-km resolution) [30] and GDAS wind vectors (6 h, 0.25° resolution) [24] for the time period June 1, 2017–May 31, 2018 are used. The GDAS dataset provides 10-m referenced ocean vector wind components (u, v), from which wind speed is derived as $(u^2 + v^2)^{1/2}$. Matchups between the two data sets are performed using a linear interpolation in time of the GDAS winds that are closest in location to CYGNSS. CYGNSS data during April 13, 2018–April 17, 2018 and January 5, 2018 are excluded due to errors in satellite calibration and file reading, respectively. Additionally, any samples with quality control flags set for the Fully Developed Seas wind speed product are excluded.

The empirical relationship between colocated wind and MSS is established using the full year of data within two control regions: [10°–25°S, 105°–120°E] and [10°–20°N, 128°–143°E]. For all analysis, MSS anomaly measurements colocated with wind speeds within 3–11 m/s are used.

Global distributions of microplastic concentration produced by the three ocean microplastic models described in [10] (1° × 1° spatial resolution) were used. The annual average global map of MSS anomaly derived from CYGNSS observations that was matched up with the microplastic concentrations was spatially averaged to the same (1° × 1°) resolution.

The van Sebille ocean microplastic concentration model shown in Fig. 1 is a single global distribution produced

at the end of a 50-year model run. It assumes sources of plastic originate along coastlines with concentrations that are proportional to human population within 200 km of the coast and scaled by each country's mismanaged waste. Plastic is advected based on particle travel probabilities calculated from a historical global set of satellite tracked drifter buoys from the NOAA Global Drifter Program, and the model does not include sinks for plastic to leave the ocean system [10].

The Lebreton model assumes sources of plastic originate at major river mouths, along coastlines, and on major shipping routes, with higher concentrations proportional to levels of human population and urban development. The source function also increases in concentration throughout its runtime based on global plastic production data. Plastics are advected based on ocean velocity fields from the HYCOM global circulation model, and the model also does not include sinks. Lebreton produces a single output of global microplastic distribution after a 30-year run time [10].

The Maximenko model assumes its plastic source is a global uniform distribution throughout the ocean. Plastic is advected using the same historical database of drifter buoys as van Sebille. Notably, unlike the other two models, the Maximenko model includes a sink mechanism that allows plastic particles to exit the system by "washing ashore" when they enter its coastal grid cells. Maximenko produces a single global microplastic distribution after a ten-year run time [10].

IV. Description of Microplastic Retrieval Algorithm

Regions of the ocean are first selected within which microplastic concentrations are believed to be low based on a global microplastic distribution model developed by van Sebille *et al.* [10]. The van Sebille model is shown in Fig. 1 with the low-concentration "control regions" highlighted. Although the equatorial latitudes in the Pacific and Atlantic Oceans are known to contain the lowest concentrations of microplastics, these regions are excluded from the partitioned regions due to the ITCZ's persistent anomalous atmospheric stability condition. Within the low-concentration control regions, CYGNSS measurements of the MSS of the ocean surface are assembled for the period June 1, 2017–May 31, 2018. Each measurement is colocated in time and space with the nearest estimate of ocean surface wind speed made by the NOAA GDAS reanalysis model. The GDAS model incorporates in situ, radar, and other satellite observations but does not use CYGNSS wind speeds [24]. Reliance on a reference wind model that does not use CYGNSS observations should help mitigate any coupling between them in the derivation of the MSS anomaly.

A density scatterplot of all (*wind speed*, *MSS*) pairs within the control regions for the year is shown in Fig. 2. The figure clearly illustrates that local wind speed is but one of several factors that controls the MSS of the ocean surface. MSS is determined by a broad range of the surface roughness spectrum, including both small (capillary) waves which are directly forced by local winds and longer (swell) waves that are highly correlated with capillary waves in an ideal, fully developed sea state, but are, in practice, only partially correlated due to dynamic ocean processes such as currents and wind speed variations [31]. The scatter seen in Fig. 2 of the samples about the best-fit line is caused by the other factors that influence the MSS. This will be shown later to introduce uncertainty into the estimation of ocean microplastic concentration.

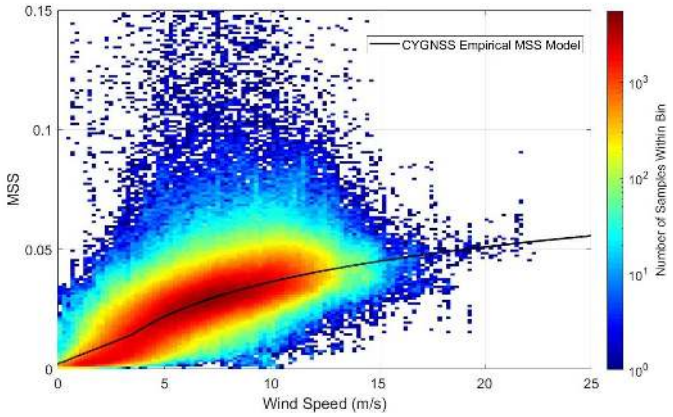

Fig. 2. Density scatterplot of ocean surface wind speed and MSS roughness for a one-year period within the control regions highlighted in Fig. 1. The solid black line is a parametric fit to the samples which provides a nominal relationship between wind speed and MSS in ocean waters with low microplastic concentration.

A least-squares parametric fit of the Katzberg empirical L-Band MSS model [32] to the samples in the scatterplot produces the following relationship:

$$\mathrm{MSS}_{\mathrm{mod}} = \begin{cases} 0.0035(U + 0.62) & \text{if } U \leq 3.49\text{m/s} \\ 0.0035(6\ln(U) - 3.39) & \text{if } U > 3.49\text{m/s} \end{cases} \quad (1)$$

where U is the ocean surface wind speed referenced to 10 m height in a neutral stability atmosphere, as reported by GDAS.

The normalized MSS anomaly at any location, either within or outside of the control regions, is defined as

$$\mathrm{MSS}_{\mathrm{anom}} = \frac{\mathrm{MSS}_{\mathrm{obs}} - \mathrm{MSS}_{\mathrm{mod}}}{\mathrm{MSS}_{\mathrm{mod}}} \quad (2)$$

where $\mathrm{MSS}_{\mathrm{obs}}$ is the MSS measured by CYGNSS and $\mathrm{MSS}_{\mathrm{mod}}$ is the MSS estimated from colocated GDAS winds using (1). $\mathrm{MSS}_{\mathrm{anom}}$ is the fractional deviation of observed from expected MSS. A normalized version of the anomaly is used so that conditions with different degrees of roughness can be directly compared. Within the control region, the expectation is that the MSS anomaly will be close to zero since the MSS model is trained using those data. Away from the control region, our hypothesis is that the MSS anomaly will become increasingly negative as greater concentrations of ocean microplastic tracers suppress the roughening of the ocean surface by surfactant wave damping.

Estimates of microplastic concentration are made from the MSS anomaly using an empirical relationship between them that is derived from a large population of colocated values. The microplastic concentration values used to train the empirical relationship are provided by the van Sebille model [10]. We choose this model because its variations in concentration

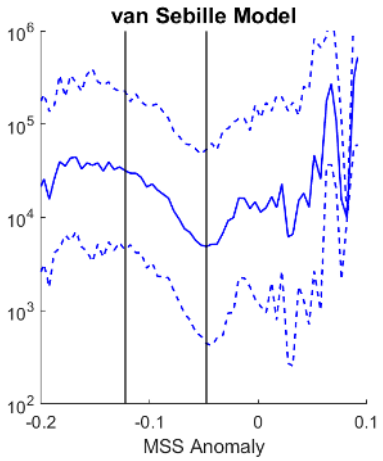

Fig. 3. Comparison between normalized MSS anomaly and microplastic number density (#/km^2) predicted by the van Sebille model using one year of MSS observations. The microplastic number density concentrations are averaged into MSS anomaly bins of 0.005 width. The region of negative anomaly between -0.1227 and -0.0478, denoted by the vertical black lines accounts for ∼61% of all samples and is used to train an empirical relationship. Standard deviation of microplastic concentrations within each bin is shown with the dashed lines. Statistics are taken with respect to $\log_{10}$(#/km^2).

have the highest correlation with the observed variations in MSS anomaly. However, the use of other models produces generally similar results, as discussed below in Section IV. Only observations within the wind speed range 3–11 m/s are used because the correlation between MSS anomaly and microplastic concentration is found to weaken at lower and higher wind speeds. The range 3–11 m/s accounts for a large majority of samples, so this restriction does not significantly reduce the sample size. MSS anomaly measurements are spatially binned into a $1^\circ \times 1^\circ$ latitude-by-longitude grid and averaged over one year. Microplastic concentration values are similarly spatially binned and the two values are compared. The comparison is shown in Fig. 3 after the microplastic number density concentrations have been averaged over MSS anomaly bin widths of 0.005 to smooth the relationship. The comparison is shown in Fig. 3. The standard deviations of binned microplastic concentrations are denoted by the dashed blue lines. The relationship can be broken up into three segments according to the number of samples that are averaged together in each MSS anomaly bin. The segment with greater than $N = 600$ samples per bin lies between MSS anomaly values of -0.1227 and -0.0478 (designated by the two vertical lines in Fig. 3). This value of N corresponds to the 95% confidence level and 4% margin of error for the average; ∼61% of all samples lie within this range of MSS anomalies. The other 39% of samples lie above and below this range. The bins with higher MSS anomalies correspond to conditions in which ocean surface roughening is more sensitive to wind forcing. The samples with lower (more negative) MSS anomalies correspond to conditions in which ocean surface roughening is highly insensitive to wind forcing. Over the central range of MSS anomalies, the relationship is quite smooth and monotonic, with increasing negative MSS anomalies generally corresponding to higher ocean microplastic concentrations. A log-linear regression is performed using the samples in the central range. The resulting relationship between plastic number density and wave damping is given by

$$\rho = 2035 \exp(-23.18\, \mathrm{MSS}_{\mathrm{anom}}) \tag{3}$$

where ρ is the number density of ocean microplastics in units of #/km^2.

TABLE I
BIAS AND RMSD COMPARISON TO REFERENCE MODELS

Product Under Test	Reference Model			
	van Sebille		Lebreton	
	Mean Diff*	RMS Diff*	Mean Diff*	RMS Diff*
van Sebille Model	--	--	0.471	0.906
Lebreton Model	-0.471	0.906	--	--
Retrieval trained with van S.	0.002	1.003	0.474	1.307
Retrieval trained with Leb.	-0.494	1.147	-0.023	1.244

*All statistics are with respect to the $\log_{10}$ (#/km^2) of the microplastic number density

V. Validation of Microplastic Retrieval Algorithm

Validation of the retrieved microplastic concentration is performed in two parts. First, estimates are compared with the original plastic concentration model with which the retrieval algorithm was trained. Since the training and validation data are the same, this is largely a consistency test of the retrieval process. The estimates are also compared with other microplastic concentration models as an independent assessment of performance. The models are also compared with one another to assess the inherent uncertainties in the models themselves. Second, the model used to train the empirical retrieval algorithm is varied and the impact that has on retrieval performance is considered. The van Sebille model was chosen as the baseline because it has the highest correlation with observed MSS anomalies, as measured by the rms difference between the model concentration and the concentration estimated from the observations. These values are labeled "rms diff" in Table I. Using the other available models has a relatively small impact on overall performance.

A. Comparison to Model Concentrations

The microplastic concentrations estimated from CYGNSS measurements vary over time and are found to have seasonal dependencies which are discussed in the following. For this reason, we compare the annual average retrieved concentrations to the van Sebille model.

A density scatterplot of model versus retrieved microplastic concentrations is shown in Fig. 4(a). The highest density of samples occurs along the 1:1 line of perfect agreement. Samples with a significant deviations from the 1:1 line may be due to retrieval errors, to variable conditions not corrected by taking a simple annual average of the retrieval, or to errors in the model itself. Note also that the model has a significantly wider dynamic range of values at the low end. Fig. 4(b) shows

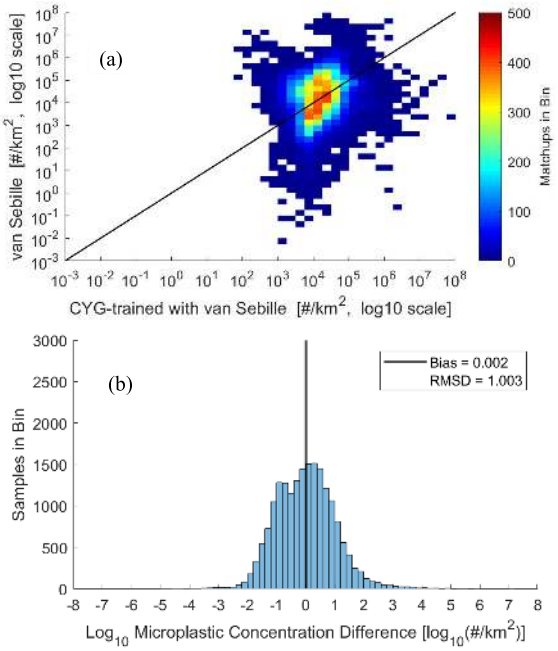

Fig. 4. (a) Density scatterplot of ocean microplastic concentration (#/km^2) retrieved by CYGNSS using an algorithm trained against the van Sebille model versus the van Sebille model values. Highest density samples occur along the 1:1 line of perfect agreement. (b) Histogram of the difference between model and retrieval. The mean difference (bias) is close to zero and the rms difference is 1.01 log$_{10}$(#/km^2).

a histogram of the difference between model and retrieval. The mean difference between model and retrieval (the retrieval bias) is 0.002, and the RMS difference is 1.003 log$_{10}$(#/km^2).

The retrieval is also compared with a model developed by Lebreton [10]. Retrieval bias and RMSD results when compared with the Lebreton model are 0.474 and 1.307 log$_{10}$(#/km^2), respectively. The bias is higher than that of the van Sebille comparison, which is to be expected since the retrieval was trained with van Sebille. The RMSD is only slightly larger in this case, suggesting that the retrieval has not been "over tuned" to one particular model. Comparing the two models to one another, their mean difference is 0.471 and their rms difference is 0.906 log$_{10}$(#/km^2). The model-to-model RMSD is slightly lower than the differences between the retrieval and either model, suggesting that most of that difference can be attributed to uncertainties in the models themselves, with a small additional component due to errors in the retrieval algorithm. The comparison statistics are summarized in Table I.

B. Dependence on Training Model

The retrieval algorithm described in Section III used the van Sebille model as its reference. A similar algorithm development is considered here using other reference models. In each case, observed MSS anomalies, averaged over one year, are colocated with the microplastic concentration predicted by the model, and a log-linear regression is performed over the same central range of MSS anomaly values within which 61% of the samples lie. This is done using the van Sebille and Lebreton models described above as well as with a third model developed by Maximenko [10]. The resulting matchups between

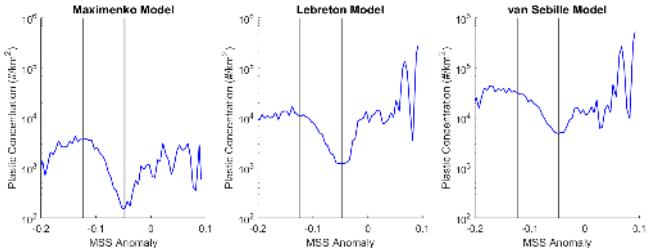

Fig. 5. Similar matchup between MSS anomaly observations and model-predicted ocean microplastic concentrations as shown in Fig. 3 for three different microplastic models. The matchup with van Sebille from Fig. 3 is included here for ease of comparison. In all three cases, the MSS anomaly agrees well with plastic concentration over the central range of values delimited by the vertical lines.

observed MSS anomalies and all three modeled microplastic concentrations are shown in Fig. 5. In each case, variations in MSS anomaly can be seen to be highly correlated with microplastic concentration, with increasing concentrations associated with increasingly negative anomalies. The physical explanation for this correlation is a reduction in the responsiveness of the ocean surface to roughening by winds that is caused either by the microplastics themselves or by some tracer (e.g., surface surfactants) with similar ocean transport behavior. A log-linear regression between the MSS anomaly and each of the three model concentrations results in Pearson correlation coefficients of 0.95 (van Sebille), 0.94 (Lebreton), and 0.92 (Maximenko). The previous validation discussion considered the case where the retrieval algorithm was trained using the van Sebille model and evaluated using the Lebreton model. The opposite test was also conducted, training with Lebreton and evaluated with van Sebille, and the comparison results are also included in Table I. In both cases, the overall retrieval performance is consistent and comparable. Comparisons involving the Maximenko model were also considered, but the results are heavily influenced by the large difference between it and the other two models. Maximenko generally predicts much lower microplastic concentrations, most likely because its model includes a sink mechanism that washes out plastics from the ocean at the coastal boundaries, whereas the other two do not.

VI. Retrieval Results

A comparison between the ocean microplastic distribution predicted by van Sebille and retrieved from MSS anomaly observations is shown in Fig. 6, together with the MSS anomaly distribution from which it was derived. An annual average of the observations is used to reduce seasonal or other time-dependent variations and more closely represent the steady-state distribution predicted by the model. In general, regions of higher and lower microplastic concentration tend to agree. In particular, the high concentration region colloquially referred to as the Great Pacific Garbage Patch, highlighted by the red box in Fig. 6, is resolved by the MSS-based retrieval. By the same token, the region bounded by the white box in the figure is associated with low predicted microplastic concentrations by the model. This region is found to have

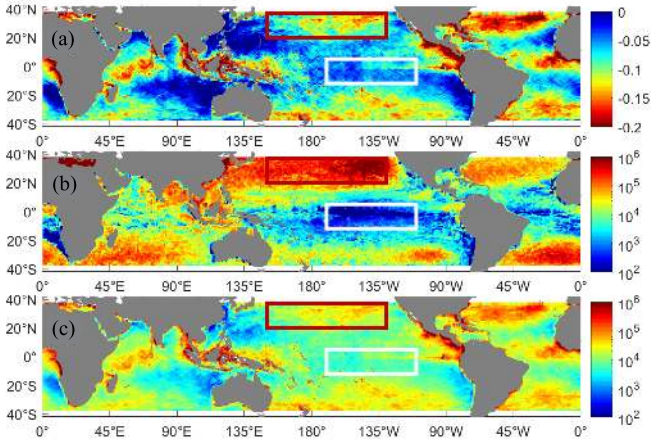

Fig. 6. Global distribution of (a) ocean MSS anomaly observations, (b) microplastic concentration (#/km^2, $\log_{10}$ scale) predicted by the van Sebille model, and (c) retrieved microplastic concentration (#/km^2, $\log_{10}$ scale) from the observations. Regions of high and low microplastic concentration are indicated by red and white boxes, respectively, and correspond to regions of large and small MSS anomaly.

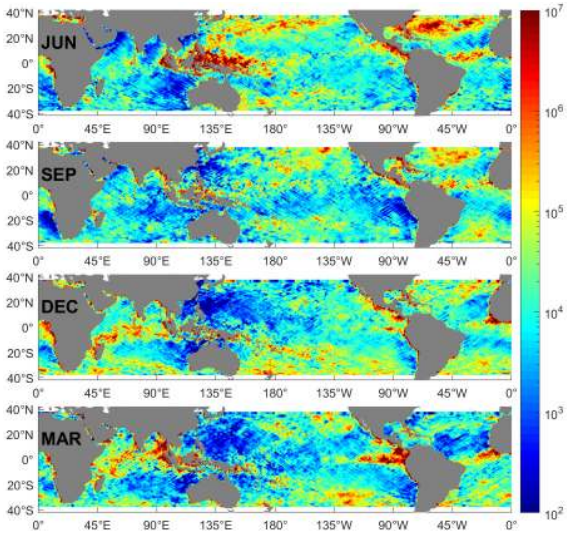

Fig. 7. Monthly average microplastic number density concentration (#/km^2, $\log_{10}$ scale) for June–September–December 2017 and March 2018. Both Atlantic and Pacific basins have generally higher concentrations in austral and boreal summer. The northern Indian Ocean has highest concentrations in the spring. These seasonal patterns tend to repeat. See Supplemental Material for a time lapse animation of the global distribution.

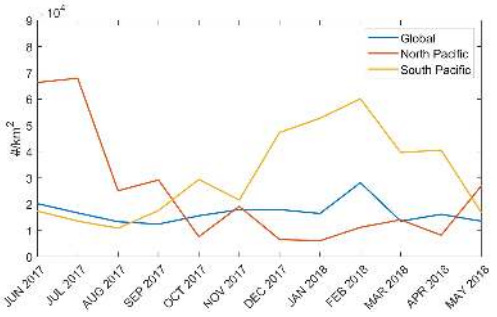

Fig. 8. Monthly average microplastic concentration (#/km^2, $\log_{10}$ scale) for the North Pacific [20°–35° N, 150° E–130° W], South Pacific [20°–35° S, 180°–100° W] and globally. Pacific mid-latitude concentrations are higher in both the boreal and austral summer, and lower in both of their winter months.

MSS anomalies near zero and correspondingly low retrieved microplastic concentrations. Note that the retrieval does suffer from over reporting of microplastics in the equatorial ITCZ. This is believed to be due to anomalous atmospheric stability conditions there, which also tend to suppress roughening. It should be noted that differences exist between the microplastic concentration estimated by the van Sebille model [Fig. 6(b)] and the concentration derived from the radar observations [Fig. 6(c)]. For example, differences can be seen in the eastern part of the Indian Ocean and near some coastlines. These discrepancies may result from uncertainties in the model or in derived concentrations.

The results in Fig. 6 are of an annual average on a global scale. Observations made on shorter temporal and finer spatial scales are considered next to examine more localized, time-dependent changes in the microplastic concentration. It is important to note that finer time and space observations will tend to increase the dynamic range of MSS anomalies compared with annual averages over global scales.

Global monthly maps of microplastic concentration for June, September, and December 2017 and March 2018 are shown in Fig. 7 to highlight seasonal changes observed in plastic distribution. Seasonal maps are averaged over 30 days with spatial resolution of 1°x 1° latitude-by-longitude, incremented by 0.25° × 0.25°. The shifts in concentration from season-to-season tend to occur gradually, as demonstrated by the time lapse video of global ocean microplastic concentration over one full year that is available in the Supplemental Material.

The strong seasonal dependence of ocean microplastic concentration at mid-latitudes in the Pacific is further illustrated in Fig. 8, which plots monthly average values for its northern [20°–35°N, 150°E–130°W] and southern [20°–35°S, 180°–100°W] segments over a full year. The time-dependent global average is also included for comparison. Concentrations in both hemispheres are highest in their respective summer months and lowest in winter. This dependence may be due to seasonal atmospheric and oceanic circulation patterns. For example, mid-latitude regions of the Pacific Ocean experience stronger currents and increased vertical mixing in the winter months of both hemispheres [33]. Increased vertical mixing would tend to decrease near-surface concentrations of microplastics and surfactants, thus reducing their wave damping effect.

Fig. 7 also illustrates the fact that microplastic concentrations in the North Indian Ocean tend to be highest in late winter/early spring and lowest in early summer. The Indian monsoon season typically extends from June to September. The Indonesia Throughflow current, which serves as the primary path for Pacific Ocean circulation into the Northern Indian Ocean, also slows significantly during the winter months due to the regional monsoon rain patterns [33]. Both of these weather patterns could be contributing to the seasonal changes observed in estimated concentration, through a combination of decreased inflow from the Pacific in the winter

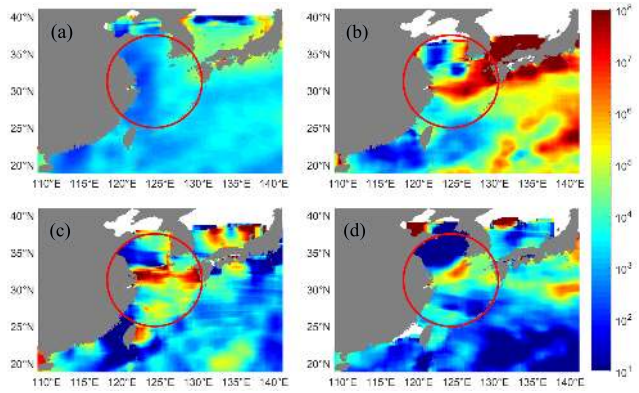

Fig. 9. Estimated microplastic outflow into the East China Sea. (a) Annual average microplastic number density concentration (#/km^2, $\log_{10}$ scale) serves as a reference. One week averages over (b) June 22, 2017–June 28, 2017, (c) October 27, 2017–November 2, 2017, and (d) December 2, 2017–December 8, 2017 reveal short lived bursts of high microplastic concentration emerging from the Qiantang (b) and Yangtze (c) and (d) River mouths and dispersing into the East China Sea in the region highlighted by red circles.

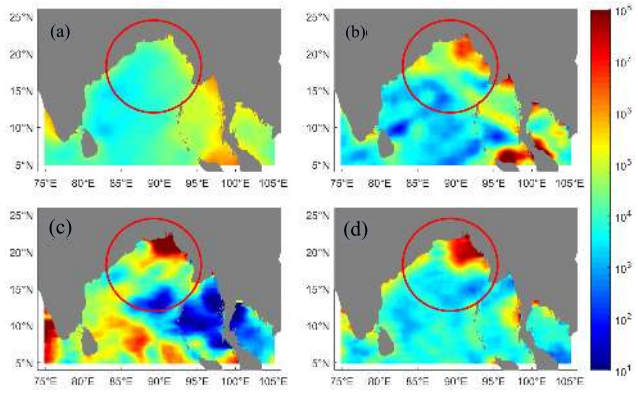

Fig. 10. Estimated microplastic outflow into the Bay of Bengal. (a) Annual average microplastic number density concentration (#/km^2, $\log_{10}$ scale) serves as a reference. One week averages over (b) August 18, 2017–August 24, 2017, (c) October 29, 2017–November 4, 2017, and (d) December 17, 2017–December 23, 2017 reveal short-lived bursts of high microplastic concentration emerging from the Ganges River mouth and dispersing into the Bay of Bengal in the region highlighted by red circles.

and increased rainwater dilution in the summer. However, these conclusions should be qualified by noting that anomalous atmospheric conditions resulting from the shifting ITCZ may also be affecting observations in the Indian Ocean.

Time lapse images of microplastic concentration on smaller spatial and temporal scales can also reveal localized sources and transport behavior. Episodic outflow events originating near Shanghai, China are highlighted in Fig. 9. Fig. 9(b)–(d) show microplastic concentrations averaged over one-week periods with spatial resolution of 2° × 2° latitude-by-longitude, incremented by 0.1° × 0.1°, in June, October, and December 2017, respectively. For reference, Fig. 9(a) shows the annual average values. The areas containing the mouths of the Yangtze and Qiantang Rivers, where they empty into the East China Sea, are highlighted by red circles in the figure. Each of the one-week averages shows evidence of outflow and dispersion from the rivers into the sea, whereas the annual average does not. In general, these outflow events tend to be short lived and so do not contribute significantly to the annual average values.

Further examples of episodic outflow events are found near the Ganges River. These are shown in Fig. 10. Fig. 10(b)–(d) exhibit plumes of high microplastic concentration from August, November, and December 2017, respectively, that originate near the mouth of the Ganges River and disperse into the Bay of Bengal. Plumes are again indicated by a red circle. Fig. 10(b)–(d) show a one-week microplastic average and use the same spatial resolution (2° × 2° latitude-by-longitude, incremented by 0.1° × 0.1°) as in Fig. 9. Areas surrounding the Ganges River mouth in the annual average map [Fig. 10(a)] remain unaffected by these outflow events.

A closer examination of the transport dynamics associated with these outflow events is possible using a Hopfmuller diagram across the East China Sea. In the diagram, microplastic concentration is averaged along the latitudinal extent of the Qiantang and Yangtze River mouths (from 31°N to 32°N) and is plotted as a function of longitude and time. The results are

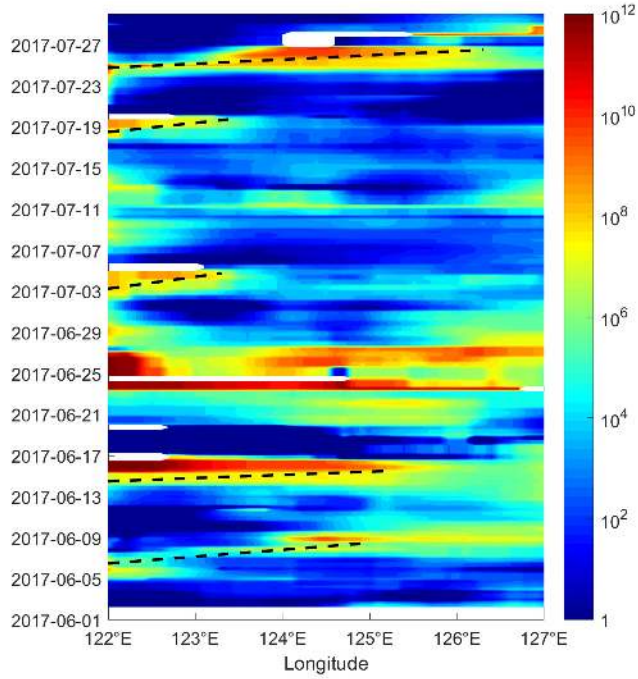

Fig. 11. Hopfmuller diagram of estimated microplastic outflow from the Qiantang and Yangtze Rivers into the East China Sea. Inclined ridges of high concentration (highlighted by dashed back lines) are indicative of west-to-east transport of the outflow. The slope of the dashed lines determines the transport velocity.

shown in Fig. 11 for June–July 2017. Transport of water with high microplastic concentration is identified in the diagram by characteristic ridges moving from west to east across the East China Sea. Several such ridges are highlighted in the figure by dashed black lines. The slope of a ridge corresponds to its transport velocity, with velocities of 0.95–3.52 m/s determined for the ones highlighted in the figure. Independent estimates of microplastic transport velocity lie in a range of 0.56–2.89 m/s [12], [34], which is generally consistent with the Hopfmuller-based estimates. The microplastic outflow

observed from the mouths of the Qiantang and Yangtze Rivers is intermittent and without a readily discernible periodicity or other pattern. The outflow events may be associated with increases in industrial production activity or in managed river discharge.

VII. Conclusion

A new method is presented for detecting and imaging ocean microplastic concentration from space using measurements of ocean surface roughness made by the CYGNSS constellation of bistatic radar receivers. The presence of microplastics is found to correlate well with the suppression of roughening of the ocean surface by winds, and the concentration of the microplastics correlates with the degree of suppression. An empirical detection algorithm is developed based on this correlative relationship, and is used to produce time lapse images of global and regional microplastic distributions that have not previously been possible. Basin scale images across the North and South Pacific Ocean resolve seasonal variations in microplastic concentration that are consistent with seasonal patterns of ocean circulation and vertical mixing. Higher resolution images on shorter time scales resolve episodic river discharge events, followed by transport across the East China Sea.

It is important to qualify these results by noting that, while there is a strong correlation between the observed MSS anomaly and modeled microplastic concentration, the retrieval algorithm developed here is empirical and may not be based on a direct physical connection between the presence of ocean microplastics and the suppression of ocean surface roughening by wind. Because the relationship used to derive the retrieval algorithm is correlative, it is possible that the roughening suppression is caused by something else that is also correlated with the presence of microplastics. One possible candidate for such an intermediary is surfactants on the ocean surface. There is evidence that they share similar transport mechanisms in the ocean as microplastics [15], and there is also evidence that they can have a damping effect on wind-driven ocean roughening [25]–[27]. These properties make surfactants a potential tracer for microplastics. Further study is needed to identify the underlying physical mechanism(s) for the roughness suppression and, if it is caused indirectly by surfactants and not directly by the microplastics themselves, to better understand how their transport mechanisms are related.

References

[1] *Plastics—The Facts 2019: An Analysis of European Plastics Production, Demand and Waste Data*, PlasticsEurope, Brussels, Belgium, 2019.

[2] M. Garside. (2019). *Global Plastic Production Statistics*. Statista. [Online]. Available: https://www.statista.com/statistics/282732/global-production-of-plastics-since-1950/

[3] J. R. Jambeck *et al.*, "Plastic waste inputs from land into the ocean," *Science*, vol. 347, no. 6223, pp. 768–770, 2015.

[4] D. K. A. Barnes, F. Galgani, R. C. Thompson, and M. Barlaz, "Accumulation and fragmentation of plastic debris in global environments," *Phil. Trans. Roy. Soc. B, Biol. Sci.*, vol. 364, no. 1526, pp. 1985–1998, Jul. 2009.

[5] M. Cole, P. Lindeque, C. Halsband, and T. S. Gallowaym, "Microplastics as contaminants in the marine environment: A review," *Mar. Pollut. Bull.*, vol. 62, pp. 2588–2597, Dec. 2011.

[6] E. J. Carpenter and K. L. Smith, "Plastics on the sargasso sea surface," *Science*, vol. 175, no. 4027, pp. 1240–1241, Mar. 1972.

[7] H. S. Auta, C. U. Emenike, and S. H. Fauziah, "Distribution and importance of microplastics in the marine environment: A review of the sources, fate, effects, and potential solutions," *Environ. Int.*, vol. 102, pp. 165–176, May 2017.

[8] C. G. Alimba and C. Faggio, "Microplastics in the marine environment: Current trends in environmental pollution and mechanisms of toxicological profile," *Environ. Toxicol. Pharmacol.*, vol. 68, pp. 61–74, May 2019.

[9] A. Cozar *et al.*, "Plastic debris in the open ocean," *Proc. Nat. Acad. Sci. USA*, vol. 111, no. 28, pp. 10239–10244, 2014.

[10] E. van Sebille *et al.*, "A global inventory of small floating plastic debris," *Environ. Res. Lett.*, vol. 10, no. 12, Dec. 2015, Art. no. 124006.

[11] M. K. Virsek, A. Palatinus, Š. Koren, M. Peterlin, P. Horvat, and A. Kržan, "Protocol for microplastics sampling on the sea surface and sample analysis," *J. Visualized Exp.*, vol. 118, no. 118, Dec. 2016, Art. no. e55161.

[12] I. Chubarenko, A. Bagaev, M. Zobkov, and E. Esiukova, "On some physical and dynamical properties of microplastic particles in marine environment," *Mar. Pollut. Bull.*, vol. 108, nos. 1–2, pp. 105–112, Jul. 2016.

[13] K. L. Law *et al.*, "Distribution of surface plastic debris in the eastern pacific ocean from an 11-year data set," *Environ. Sci. Technol.*, vol. 48, no. 9, pp. 4732–4738, May 2014.

[14] T. Kukulka, G. Proskurowski, S. Morét-Ferguson, D. W. Meyer, and K. L. Law, "The effect of wind mixing on the vertical distribution of buoyant plastic debris," *Geophys. Res. Lett.*, vol. 39, no. 7, Apr. 2012, Art. no. L07601.

[15] E. van Sebille *et al.*, "The physical oceanography of the transport of floating marine debris," *Environ. Res. Lett.*, vol. 15, no. 2, pp. 1–32, Feb. 2020, doi: 10.1088/1748-9326/ab6d7d.

[16] M. Nikolai *et al.*, "Toward the integrated marine debris observing system," *Frontiers Mar. Sci.*, vol. 6, p. 447, Aug. 2019. [Online]. Available: https://www.frontiersin.org/article/10.3389/fmars.2019.00447, doi: 10.3389/fmars.2019.00447.

[17] S. Serranti, R. Palmieri, G. Bonifazi, and A. Cózar, "Characterization of microplastic litter from oceans by an innovative approach based on hyperspectral imaging," *Waste Manage.*, vol. 76, pp. 117–125, Jun. 2018.

[18] C. S. Ruf *et al.*, "New ocean winds satellite mission to probe hurricanes and tropical convection," *Bull. Amer. Meteorolog. Soc.*, vol. 97, no. 3, pp. 385–395, Mar. 2016, doi: 10.1175/BAMS-D-14-00218.1.

[19] M. P. Clarizia and C. S. Ruf, "Wind speed retrieval algorithm for the cyclone global navigation satellite system (CYGNSS) mission," *IEEE Trans. Geosci. Remote Sens.*, vol. 54, no. 8, pp. 4419–4432, Aug. 2016, doi: 10.1109/TGRS.2016.2541343.

[20] F. J. Wentz and D. K. Smith, "A model function for the ocean-normalized radar cross section at 14 GHz derived from NSCAT observations," *J. Geophys. Res.*, vol. 104, no. 5, pp. 11499–11514, 1999.

[21] C. S. Ruf and R. Balasubramaniam, "Development of the CYGNSS geophysical model function for wind speed," *IEEE J. Sel. Topics Appl. Earth Observ. Remote Sens.*, vol. 12, no. 1, pp. 66–77, Jan. 2019.

[22] H. Hersbach, "Assimilation of scatterometer data as equivalent-neutral wind," European Center Medium Range Weather Forecasting, Reading, U.K., Tech. Memo. 629, 2010.

[23] C. S. Ruf *et al.*, "A new paradigm in Earth environmental monitoring with the CYGNSS small satellite constellation," *Sci. Rep.*, vol. 8, no. 1, p. 8782, Dec. 2018.

[24] *National Centers for Environmental Information, NCEI DSI 6172, NOAA*, NCEI/NOAA, Silver Spring, MD, USA, 2018.

[25] W. Alpers and H. Hühnerfuss, "The damping of ocean waves by surface films: A new look at an old problem," *J. Geophys. Res.*, vol. 94, no. 5, pp. 6251–6265, 1989.

[26] D. Kiefhaber, C. J. Zappa, and B. Jahne, "Influence of natural surfactants on short wind waves in the coastal Peruvian waters," *Ocean Sci. Discuss.*, vol. 12, no. 4, pp. 1291–1325, 2015.

[27] B. Spivak, J.-M. Vanden-Broeck, and T. Miloh, "Free-surface wave damping due to viscosity and surfactants," *Eur. J. Mech.-/Fluids*, vol. 21, no. 2, pp. 207–224, Jan. 2002.

[28] E. A. D'Asaro *et al.*, "Ocean convergence and the dispersion of flotsam," *Proc. Nat. Acad. Sci. USA*, vol. 115, no. 6, pp. 1162–1167, Feb. 2018.

[29] Y. Xia, X.-M. Xiang, K.-Y. Dong, Y.-Y. Gong, and Z.-J. Li, "Surfactant stealth effect of microplastics in traditional coagulation process observed via 3-D fluorescence imaging," *Sci. Total Environ.*, vol. 729, Aug. 2020, Art. no. 138783.

[30] CYGNSS. (2018). *CYGNSS Level 2 Science Data Record Version 2.1. Ver. 2.1. PO.DAAC, CA, USA. Dataset*. Accessed: Dec. 12, 2018. [Online]. Available: https://doi.org/10.5067/CYGNS-L2X21

[31] V. U. Zavorotny and A. G. Voronovich, "Scattering of GPS signals from the ocean with wind remote sensing application," *IEEE Trans. Geosci. Remote Sens.*, vol. 38, no. 2, pp. 951–964, Mar. 2000, doi: 10.1109/36.841977.

[32] S. J. Katzberg, O. Torres, and G. Ganoe, "Calibration of reflected GPS for tropical storm wind speed retrievals," *Geophys. Res. Lett.*, vol. 33, no. 18, Sep. 2006, Art. no. L18602.

[33] J. Callies, R. Ferrari, J. M. Klymak, and J. Gula, "Seasonality in submesoscale turbulence," *Nature Commun.*, vol. 6, no. 1, p. 6862, Nov. 2015.

[34] H. Zhang, "Transport of microplastics in coastal seas," *Estuarine, Coastal Shelf Sci.*, vol. 199, pp. 74–86, Dec. 2017.

Madeline C. Evans received the B.S.E. degree *(cum laude)* in electrical engineering and the B.S. degree in German from the University of Michigan, Ann Arbor, MI, USA, both in 2020.

During her undergraduate studies, she was involved in community projects as a part of Epsilon Eta, a professional environmental fraternity at the University of Michigan. In 2016, she became the youngest person to participate in the Academic Year in Freiburg program. At Albert Ludwigs University of Freiburg, Freiburg im Breisgau, Germany, her German studies were focused on renewable energy and sustainability topics. She is interested in merging her background skills in signal processing and control systems with her interest in Earth science and sustainability. She is a Research Assistant with the Department of Climate and Space Sciences and Engineering, University of Michigan. She primarily works on remote detection of microplastics via the NASA Cyclone Global Navigation Satellite System. Her research interests include GNSS-R remote sensing, remote sensing of pollutants, and signal processing algorithm development.

Mr. Evans has previously presented at the American Geophysical Union (AGU) Fall conference in 2019 and participated in the European Geophysical Union (EGU) conference in 2020.

Christopher S. Ruf (Fellow, IEEE) received the B.A. degree in physics from Reed College, Portland, OR, USA, in 1982, and the Ph.D. degree in electrical and computer engineering from the University of Massachusetts at Amherst, Amherst, MA, USA, in 1987.

He has worked previously at Intel Corporation, Mountain View, CA, USA, Hughes Space and Communication, El Segundo, CA, USA, the NASA Jet Propulsion Laboratory, Pasadena, CA, USA, and Pennsylvania State University, University Park, PA, USA. He is the Frederick Bartman Collegiate Professor of climate and space science with the University of Michigan, Ann Arbor, MI, USA, and a Principal Investigator of the NASA Cyclone Global Navigation Satellite System mission. His research interests include GNSS-R remote sensing, microwave radiometry, atmosphere and ocean geophysical retrieval algorithm development, and sensor technology development.

Dr. Ruf is a member of the American Geophysical Union (AGU), the American Meteorological Society (AMS), and Commission F of the Union Radio Scientifique Internationale. He is a former Editor-in-Chief of the IEEE TRANSACTIONS ON GEOSCIENCE AND REMOTE SENSING and has served on the editorial boards of the *Radio Science* and *the Journal of Atmospheric and Oceanic Technology*. He was a recipient of four NASA Certificates of Recognition and seven NASA Group Achievement Awards, as well as the 1997 TGRS Best Paper Award, the 1999 IEEE Resnik Technical Field Award, the 2006 IGARSS Best Paper Award, and the 2014 IEEE GRSS Outstanding Service Award.